THE JOURNAL OF PHYSICAL CHEMISTRY B

ARTICLE

pubs.acs.org/JPCB

Solubilization of Gabapentin into H_{II} Mesophases

Ben Achrai, Dima Libster, Abraham Aserin, and Nissim Garti*

Casali Institute of Applied Chemistry, The Institute of Chemistry, The Hebrew University of Jerusalem, Edmond J. Safra Campus, Givat Ram, Jerusalem 91904, Israel

ABSTRACT: In the present work, we report on the solubilization of gabapentin (GBP) into lyotropic hexagonal mesophases composed of monoolein, tricaprylin, and water. It was demonstrated that the hexagonal structure remained intact up to 2 wt % gabapentin, whereas the lamellar phase coexisted with the hexagonal one in the concentration range of 3−4 wt % of the drug. At gabapentin content of 5−6 wt %, only lamellar phases containing defects such as dislocations and multilamellar vesicles were detected. Incorporation of GBP decreased the lattice parameter of the H_{II} mesophase from 56.6 to 50.6 Å, while the structural dimensions of the lamellar phase were not affected. ATR−FTIR analysis suggested enhanced hydrogen bonding between the protonated amine of GBP and the O−H groups of the GMO and the water surrounding in the inner hydrophilic interface region. This led to intercalation of the drug into the water−lipid interface. At higher GBP loads of 4−6 wt %, thermal analysis revealed disordering within the lipid packing, apparently induced by the spatially altered interface area. Rheological measurements correlated the macroscopic features of the systems with alterations on the molecular level and allowed distinguishing between closely related mesophases due to their different rheological characteristics. In vitro transdermal delivery studies showed that the examined mesophases enabled a sustained release of GBP compared to its aqueous solution. Sustained release was more pronounced in the case of the hexagonal mesophase, compared to the lamellar one.

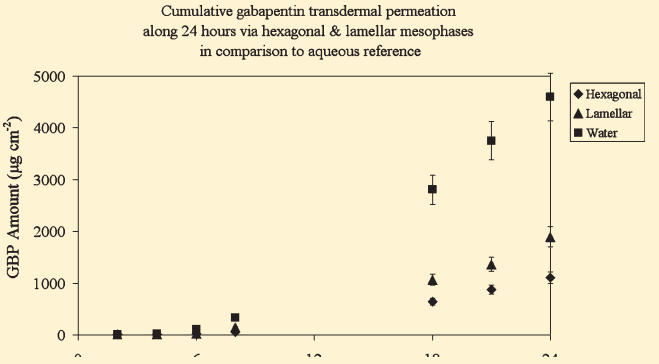

INTRODUCTION

Lyotropic liquid crystals (LLCs) have been subjected to extensive scientific research in the last few decades due to their numerous potential applications such as templates for synthesis,[1] polymerization,[2] crystallization,[3,4] composing food systems,[5] and shielding against degradation processes.[6] These systems also showed great potential as delivery carriers of small bioactive compounds such as amino acids, drugs,[7,8] vitamins,[9] and peptides,[10,11] as well as macromolecules such as proteins and enzymes.[4,6,12−16]

Glycerol monooleate (GMO, monoolein) is a polar lipid that is commonly used as a food emulsifier. Presently, GMO is the preferred amphiphile for formulating LLC phases for drug delivery. This is a nontoxic, biocompatible, and biodegradable lipid that possesses low water solubility but swells and forms several liquid crystalline phases in excess water. Suitable rheological properties,[10,11] biocompatibility, high solubilization capacity, and substrate diversity of the LLCs made them promising controlled-release drug delivery vehicles for oral and transdermal administration.[17]

Among the abundant LLCs studied, there are lamellar L_α (planar or vesicular such as unilamellar vesicles, ULVs, and multilamellar vesicles, MLVs—both may be denoted as liposomes), hexagonal (normal, H_I, or inverted H_{II}), and normal or inverted cubic (bicontinuous or micellar) structures.[18−22] Additional less common structures such as sponge phases were investigated as well.[17] The H_{II}LCs exhibit a 2D order of tightly packed and infinite straight water-filled rods composing a hexagonal lattice.[23,24] These mesophases were shown to incorporate hydrophilic additives within their aqueous domains. Likewise, hydrophobic compounds can be incorporated within the lipophilic space,[18] in which the lipids are radially oriented outward from the channels' perimeters. Amphiphilic molecules may also reside within the interface area in an adjusted direction, depending on guest molecule chemical nature.[6,11] Inverted hexagonal mesophase morphology resembles vertebrates cell membranes at the time of (clathrin-mediated) endocytosis[25,26] and have proper viscoelastic properties for the aforementioned routes of administration, in comparison to the more rigid cubic phases[19,27] or to the more loosely packed lamellar phases.[28] Furthermore, H_{II} mesophases were found to serve as release-rate regulators for several nutraceuticals[9,10] and pharmaceuticals[7,29] in transdermal permeation, having the ability to enhance or delay the diffusion rate codepending on the delivered substance's chemical nature and therapeutic doses.

The H_{II} mesophase based on GMO and water is only stable at a narrow temperature range of 85−95 °C. The addition of low

Received: September 15, 2010
Revised: October 26, 2010
Published: December 23, 2010

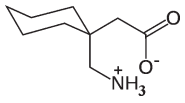

Figure 1. Molecular structure of gabapentin in neutral pH.

concentrations (4−13.5 wt %) of C_8-triglyceride tricaprylin (TAG) to the binary mixture led to stabilization of the hexagonal structure at 13 °C and up to ca. 75 °C.[30] The physical properties of the ternary H_{II}LCs were extensively studied.[31] In addition, several hydrophilic (proline, ascorbic acid, desmopressin), lipophilic (tocopherol, cyclosporine A), and amphiphilic (ascorbyl palmitate, tocopheryl acetate) biomolecules were solubilized into the subjected mesophases.[9,10,23,29,32] The structural effects and molecular interactions upon bioadditive incorporation were examined in detail as well.

Gabapentin (GBP) is a generic γ-aminobutyric acid (GABA) analogue with an advanced designed C_β incorporated cyclohexane ring for enhanced diffusion across the blood−brain barrier (Figure 1). GBP is a low molecular weight drug (171.2 g/mol) present in its zwitterion form and averages approximately 10 wt % solubility at pH 7.

Gabapentin displays approved efficacy against epilepsy,[33] postherpetic neuralgia,[34] diabetic neuropathy,[35,36] hot flashes,[37] restless legs syndrome,[38] anxiety disorders,[39] nystagmous,[40,41] and narcotics withdrawal.[42,43] The mechanism of action of this drug has not been fully revealed, but it was shown that GBP acts by binding to the $\alpha_2\delta$ subunit of a voltage-dependent calcium channel,[44,45] contrary to its initial objective—to mimic GABA activity.[46]

The remedy is administered orally and absorbed into the bloodstream through a low-capacity solute L-amino acid transporter that is mainly situated in the upper small intestine.[47] The L-transporter regularly passes bulky hydrophobic amino acids such as phenylalanine and leucine. GBP peaks in serum within 1−2 h after ingestion are not metabolized in the liver and do not bind plasma proteins. Ultimately, the drug is eliminated by renal excretion with a short half-life of 5−7 h,[48] necessitating ingestion three to four times per day, which may lead to noncompliance in individuals with epilepsy.[49] Nonetheless, an absorption deficiency occurs due to transport system saturation with escalating doses. Drug bioavailability is dose-dependent and drops from ∼60% at a 300 mg dose to ∼35% or less at the 1600 mg therapeutic dose, sufficient to treat various neuropathy disorders such as peripheral diabetic neuropathy pain.[36,48] Furthermore, intestinal expression of the L-transporter is subject to significant individual expression variations. As a result, there is a broad range of gabapentin absorption difference in people suffering from epilepsy, postherpetic neuralgia, and diabetic neuropathy.[36,49,50]

In the present study, we attempted to overcome gabapentin pharmacokinetic restraints by introducing the drug into a GMO/H_2O/TAG-based H_{II}LC vehicle. In that manner, GBP can be released in a controlled way to prevent intestinal L-transporter capacity saturation and lower the drug's side effects. Moreover, topical transdermal administration may relieve peripheral neuropathy with avoidance of systemic side effects. To fulfill these objectives to their fullest extent, a fundamental comprehensive study of the GBP concentration-dependent LLCs must be initially implemented by means of structure and chemical interaction characterizations. Structural identification was performed by polarized light microscopy and SAXS. Molecular interactions of the guest molecule with the structures' comprising compounds were examined by ATR−FTIR spectroscopy and DSC analysis. The macroscopic interrelation of the obtained GBP-modified mesophases was explored by rheological experiments. In addition, the in vitro system of Franz diffusion cells was utilized to investigate the applicability of transdermal delivery of gabapentin via the obtained drug concentration-dependent mesophases.

EXPERIMENTAL METHODS

Materials. Gabapentin powder (form II) was a kind gift from AZR Chemicals (Netanya, Israel). Monoolein, GMO, distilled glycerol monooleate (min. 97.1 wt % monoglyceride, 2.5 wt % diglyceride, and 0.4 wt % free glycerol; acid value 1.2, iodine value 68.0, melting point 37.5 °C) was purchased from Riken Vitamin Co. (Tokyo, Japan). Tricaprylin (TAG) (99%) was obtained from Sigma Chemical Co. (St. Louis, MO, USA). D_2O (D, 99.9%), was purchased from Cambridge Isotope Laboratories, Inc. (Andover, MA, USA). Hydrochloric acid 1 M was purchased from Belgar Inc. (Jerusalem, Israel). Sodium hydroxide 1 M was purchased from Mallinckrodt Baker (Deventer, Holland). 1-Fluoro-2,4-dinitrobenzene (FDNB, 99%) was purchased from Alfa Aesar (Ward Hill, MA, USA). Phosphate-buffered saline (PBS) was purchased from Biological Industries (Kibbutz Beit Haemek, Israel). Boric acid (C.P.) and potassium chloride (A.R.) were obtained from Frutarom (Haifa, Israel). Sodium phosphate monobasic (A.R.) was obtained from Mallinckrodt Baker (Paris, KY, USA). Acetonitrile (HPLC grade) was purchased from Mallinckrodt Baker (Phillipsburg, NJ, USA). The water was double distilled. All ingredients were used without further purification.

Sample Preparation. An H_{II}LC system composed of GMO, 72 wt %, TAG, 8 wt %, and water, 20 wt %, was chosen to be the starting assembly for the solubilization experiments. First, weighed quantities of GBP (1−10 wt %) were dissolved in weighed amounts of H_2O in sealed glass tubes, and then the aqueous solutions were mixed with weighed quantities of a preheated (ca. 40 °C) lipid phase made of GMO and TAG in a ratio of 1:9. A nitrogen atmosphere was implemented to avoid GMO oxidation. Then the mixtures were heated to ca. 75 °C and ultimately slightly stirred. All samples were left to equilibrate at 25 ± 0.5 °C for 24 h and were found to remain stable for at least six months (supports for this claim were obtained by repeatable polarized light microscope images and SAXS measurements). It should be mentioned that the H_2O/GMO/TAG wt % ratio remained fixed, while their overall wt % progressively decreased.

Methods and Instrumentation. *Polarized Light Microscopy.* Samples were inserted between two glass microscope slides and observed with a Nikon light microscope Eclipse 80i (Tokyo, Japan) model equipped with cross-polarizers and attached to a digital Nikon DXM 1200C camera and a PC monitor. The samples were analyzed at room temperature.

Small-Angle X-ray Scattering (SAXS). Scattering measurements were performed using Cu Kα radiation (λ = 0.154 nm) from a Rigaku RA-MicroMax 007 HF X-ray generator operated at a power rating up to 1.2 kW generating a 70 × 70 mm^2 spot size and focus. The direct beam then went through a vacuum Osmic CMF12-100CU8 focus unit with a beam size at the sample position of 0.7 × 0.7 mm^2. The scattered beam went through a flight path filled with He and reached a Mar345 Image Plate detector. The samples were inserted into 1.5 mm quartz capillaries that were then flame-sealed. The temperature was maintained at 25 ± 1 °C with an exposure time of ca. 20 min. The sample to detector distance was calibrated using silver behenate.

Wide-Angle X-ray Scattering (WAXS). Scattering measurements were performed on a Philips PW 1710 diffractometer with parallel-beam optics, 2° Soller slits for incident and diffracted beams, and 0.2 mm receiving slits. Monochromated Cu Kα radiation was used. LLCs containing crystallized GBP were mounted on low-background quartz sample holders. XRD patterns were recorded in 6°−40° 2θ scale range at room temperature, 40 kV tube voltage, 35 mA tube current, and step scan mode with a scanning rate of 0.02° 2θ s^{-1}.

Attenuated Total Reflectance−Fourier Transform Infrared (ATR−FTIR) Measurements. An Alpha P model spectrometer, equipped with a single reflection diamond ATR sampling module, manufactured by Bruker Optik GmbH (Ettlingen, Germany), was used to record the FTIR spectra. The spectra were recorded with 50 scans, at 25 °C; a spectral resolution of 2 cm^{-1} was obtained.

ATR−FTIR Data Analysis. MultiGaussian fitting has been utilized to resolve individual bands in the spectra. The peaks were analyzed in terms of peak frequencies, width at half-height, and area. The ATR−FTIR measurements were conducted with D_2O replacing the water to avoid a hydroxyl stretching band overlapping with the GMO hydroxyl bands.

To resolve the spectra of the protonated amine and the carboxylate bands of the guest molecule, the drug was dissolved in acidic (pH 0), neutral (pH 7), and alkaline (pH 14) aqueous solutions. The pH was adjusted by adding hydrochloric acid or sodium hydroxide to the neutral solution. pK_a(carboxylate) = 4 and pK_a(amine) = 10; hence, in pH 0 the carboxylate is unionized (COOH) and the amine is protonated (NH_3^+). In pH 7 the drug is in its zwitterion state, and in pH 14, the carboxylate is ionized (COO^-) and the amine is neutral (NH_2). With this information in mind, we could attribute the COO^- and NH_3^+ obtained bands by monitoring the shifting, appearance and disappearance of specific bands in the different pH aqueous solutions; e.g., the NH_3^+ rocking band[51] appeared in pH 0 at 1535 cm^{-1}, shifted downward to 1517 cm^{-1} in pH 7, and disappeared in pH 14. The same procedure was executed to determine the carboxylate symmetric and asymmetric stretching bands.

Differential Scanning Calorimetry (DSC). A Mettler Toledo DSC822 (Greifensee, Switzerland) calorimeter was used. The DSC measurements were carried out as follows: 5−10 mg of LLC samples was weighed using a Mettler M3 microbalance in standard 40 μL aluminum pans and immediately sealed by a press. The samples were rapidly cooled in liquid nitrogen from 25 °C to −40 °C, at a rate of −10 °C min^{-1}, remained there for 30 min, and eventually were heated at 1 °C min^{-1} to 40 °C. An empty pan was used as a reference. The instrument determined the fusion temperatures of the solid components and the total heat transferred in any of the observed thermal processes. The enthalpy change associated with each thermal transition was obtained by integrating the area of the relevant DSC peak. DSC temperatures reported here were reproducible to ±0.5 °C.

Rheology Measurements. Rheological measurements were performed using the Rheoscope 1 rheometer (Thermo-Haake, Karlsruhe, Germany). A cone−plate sensor was used with a diameter of 35 mm, cone angle of 1°, and a gap of 0.024 mm. The linear viscoelastic range (LVR) of a material was determined before carrying out the oscillatory measurements. The storage and loss moduli were plotted as a function of stress at ω = 1 Hz and T = 25 ± 0.2 °C (data not shown). With GBP loads of 0−4 wt %, the shear moduli were independent of stress up to a critical applied stress and generally were observed to fall off sharply beyond the values of 100−120 Pa. These results indicate that the samples possess linear viscoelastic properties up to about 100−120 Pa. Above these typical values, the microstructure of the LLC phases breaks down, as reflected by the rapid decrease of the moduli. With GBP loads of 5−6 wt %, the LVR region was held up to only 10 Pa. According to the determined LVRs, the viscoelasticity measurements of samples with 0−4 wt % GBP were generally performed at 75 Pa. Samples with 5−6 wt % GBP were measured at 1 Pa. Frequency-dependent rheological measurements were conducted in the range of 0.1−100 rad s^{-1}. The viscoelasticity of the LLC phases was characterized in terms of the elastic modulus G', the loss modulus G'', the complex viscosity η^*, and the longest relaxation time τ_{max}, according to the Maxwell model. All tests were run in triplicate and found to be reproducible.

In Vitro Transdermal Permeation Studies. *Experimental Procedure.* The permeability of gabapentin through porcine skin was determined in vitro with a Franz diffusion cell system (PermeGear Inc., Hellertown, PA, USA). The porcine skin was obtained by peeling from ears of butchered white pigs by careful dissection and dermatomization processes that took place in The Institute of Animal Research (Kibbutz Lahav, Israel). The skin strips were stored at −20 °C and used within a month. Before the experiments, the skin was thawed and lifted on Franz cells with a diffusion area of 0.635 cm^2, with the stratum corneum facing the donor compartment. The receptor compartment was filled with PBS (pH 7.2) and kept under constant stirring at 37 ± 0.5 °C. An amount of 100 mg of the liquid crystalline formulations (2 and 6 wt % GBP) or water solution (10 wt % GBP) was applied to the surface of the stratum corneum. Samples (500 μL) were drawn simultaneously from each receptor compartment at constant time periods.

Analytical Method. *Gabapentin Derivatization.* Precolumn derivatization with 1-fluoro-2,4-dinitrobenzene (FDNB) was carried out prior to the chromatography process, following a reported procedure.[52] The filtered samples were derivatized by introduction to 0.25 M borate buffer prepared by dissolving appropriate quantities of boric acid and potassium chloride in water and adjusting the pH to 8.2 by addition of 1 M NaOH. Then, the borate-diluted samples were mixed with FDNB dissolved in acetonitrile. The mixtures were heated to ca. 65 °C for 10 min in the dark, cooled to room temperature, and eventually quenched with 1 M HCl. The calibration curve was set by standard solutions (prepared in the same manner).

Chromatographic Conditions. Gabapentin content in the samples was determined by a high-performance liquid chromatography (HPLC, Waters 600 series, Milford, MA, USA) apparatus equipped with a photodiode array detector (Waters 996) and autosampler (Waters 717plus). Isocratic elution was carried out with aqueous 50 mM NaH_2PO_4 (pH = 2.5) and acetonitrile (30:70, v/v). The wavelength for UV detection was 360 nm. The column used was Luna 5 μm, C_{18}, 250 mm × 4.6 mm (Phenomenex, Torrance, CA). The chromatography was performed at room temperature at a flow rate of 1 mL min^{-1}. The injection volume was 40 μL, and the retention time of the drug was 8 min.

In Vitro Data Calculation. The cumulative drug permeation (Q_t) was calculated with regard to the continuous dilutions from the following equation.

$$Q_t = V_r C_t + \sum_{i-0}^{t-1} V_s C_i$$

dx.doi.org/10.1021/jp108801d | J. Phys. Chem. B 2011, 115, 825–835

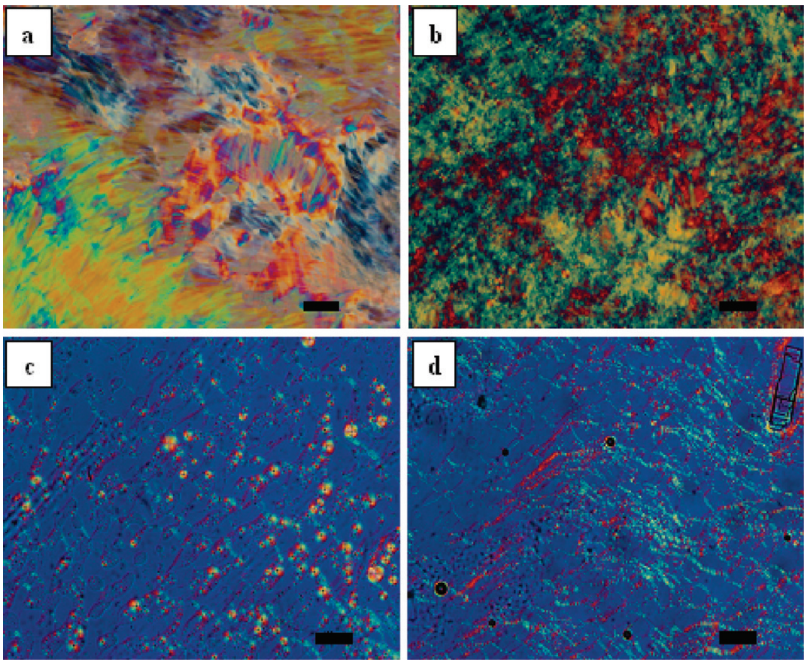

Figure 2. Polarized light microscope images obtained for gabapentin contents of (a) 2 wt %, (b) 4 wt %, (c) 6 wt %, and (d) 8 wt %. The scale bar is 100 μm.

where C_t is the drug concentration of the receiver solution at each sampling time; C_i is the drug concentration of the ith sample; and V_r and V_s are the volumes of the receiver solution and the sample, respectively. The obtained data were expressed as the cumulative drug permeation per unit of skin surface area, Q_t/S, as function of time. The steady-state fluxes (J_{ss}) were calculated by linear regression interpolation of the experimental data: $J_{ss} = \Delta Q/\Delta tS$.

RESULTS AND DISCUSSION

Gabapentin Solubilization and Structure Characterization. *Polarized Light Microscopy (PLM).* Preliminary structure examination through a cross-polarized light microscope was implemented to distinguish between typical mesophases according to their characteristic textures.[30] With GBP concentrations of 0−4 wt %, a fanlike texture was observed, indicating formation of a hexagonal mesophase (Figure 2a−d). At 5−6 wt % of drug loads, a texture of "mosaic-like" spread strips accompanied by "onion-like" clusters was observed, indicating a transition to a distorted lamellar mesophase containing MLVs and local defects within. At higher loading concentrations (7−10 wt % GBP), the mosaic-like texture was accompanied by additional polygonal shapes, suggesting crystallized precipitations.

SAXS Measurements. Further structure clarification was conducted by SAXS measurements to distinguish the different LLCs by their Bragg peak d-spacing ratios. Likewise, the lattice parameter α, which represents the smallest periodic unit from which the LLC can be built, was calculated.[30] With initial GBP concentrations of up to 2 wt %, homogeneous hexagonal structure was maintained with a decrease of 6 Å in the lattice parameter (Figure 3). With 3−4 wt % of drug solubilized, a lamellar mesophase appeared, coexisting with the preceding hexagonal one. The hexagonal lattice parameter increased by 2.3 Å, and the lamellar lattice parameter was calculated to be 43.9 ± 1 Å. At 5−6 wt % GBP incorporated, a homogeneous lamellar mesophase emerged with a near constant lattice parameter of 43.6 ± 1 Å.

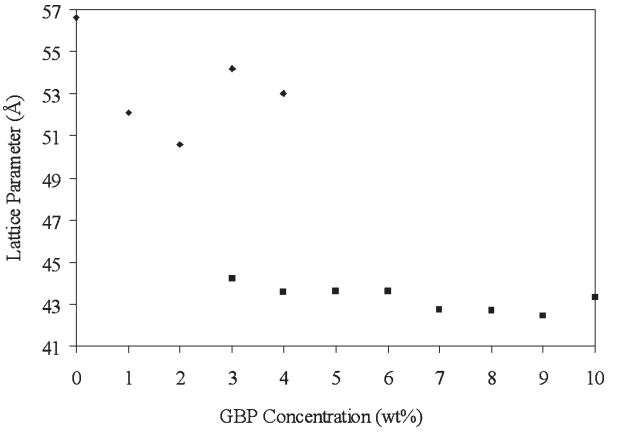

Figure 3. Mesophase characteristic lattice parameter as a function of gabapentin content: ■, L_α; ◆, H_{II}.

At greater concentrations of the guest molecule (7−10 wt %), crystalline precipitations were confirmed by WAXS analysis (data not shown), in addition to the lamellar structure. The L_α lattice parameter was around 43 ± 1 Å. Thus, within the range where the hexagonal structure was formed (1−4 wt % GBP), at low drug concentrations (1−2 wt %), GBP acted as a kosmotrope. In contrast, with moderate drug loads (3−4 wt %), gabapentin demonstrated a chaotropic behavior.[10,53] It is reasonable to assume that with 1−2 wt % of drug solubilized the obtained trend is due to partial dehydration of the GMO hydroxyls caused by the guest molecule polar groups' interactions. On the contrary, a possible intercalation of the drug between the surfactant headgroups ruled the obtained course with moderated GBP loads (3−4 wt %) to form a lamellar mesophase. The rationale for the latter trend can be easily understood by the change in the critical packing parameter (CPP). The CPP describes the geometric features of the surfactant and its relation

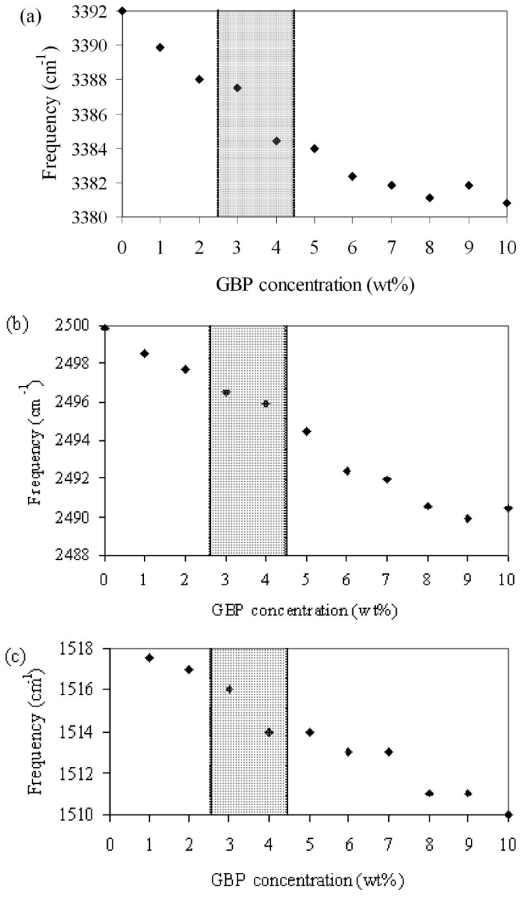

Figure 4. Stretching frequency of (a) O−H of GMO and (b) O−D of D_2O as a function of gabapentin content. (c) Rocking frequency of $N-H_3^+$ as a function of gabapentin content.

to the obtained self-assembled structure morphology.[54] CPP = V_0/a_0l where V_0 is the lipid volume; a_0 is the polar headgroup cross-section area; and l represents the tail length. A typical CPP value of ~1.7 is characteristic of H_{II} structure, whereas CPP ≈ 1 is characteristic of the lamellar structure. As stated, with moderate drug loads, GBP increased the cross-section area of the GMO polar headgroups and decreased the CPP value, which is evidenced by the transition to the lamellar structure.

At this stage, with combined PLM−SAXS−WAXS analysis, it was confirmed that with increasing drug loads GBP induced $H_{II}-L_\alpha$ transition, whereas maximum drug solubilization was achieved at 6 wt %.

Investigation of GBP Interactions within the LLC Structures. *ATR−FTIR.* ATR−FTIR analysis was performed to determine the localization of the drug within the structure by correlating its molecular interactions with the comprising components. The LLC structure vibrational changes were assigned to three main regions within the mesophase: water channels, surfactant interface, and lipid-rich.

Water channel region represents the bulk water and the inner hydrophilic interface assembled by the GMO headgroups' hydroxyls and bound water molecules. With increasing concentrations of the solubilized drug, there was a significant drop in the stretching frequency of the surfactant headgroups' O−H bond (Figure 4a). A similar red-shift tendency was obtained for the stretching frequency of the O−D bond of D_2O and for the bending frequency of the NH_3^+ bond of GBP (Figure 4b,c). In addition, the

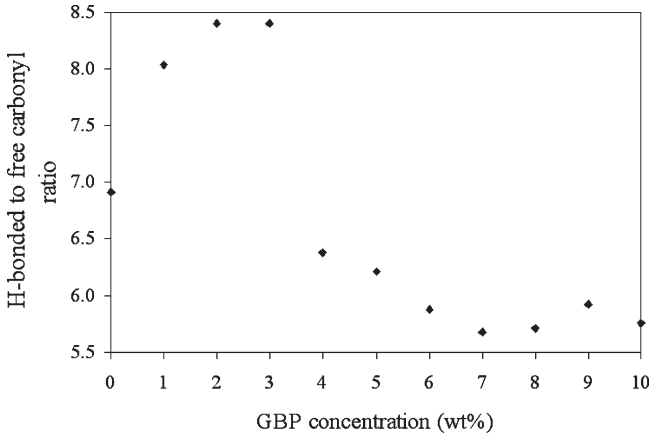

Figure 5. Peak area ratio of the H-bonded carbonyl group to the free carbonyl group measured after Gaussian fitting, as a function of gabapentin content.

asymmetric and symmetric stretching frequencies of the COO^- bond of GBP's carboxylate had a diminutive decrease of 3 cm^{-1} from 1570 to 1567 ± 1 and from 1400 to 1397 ± 1 cm^{-1}, respectively. This trend of decreasing frequencies indicates stronger hydrogen bonding between the surfactant and D_2O hydroxyls and GBP hydrophilic functional groups. We can assume that with increasing loads the drug is gradually integrated into the water channels' interface.

Surfactant interface region can be divided into two subregions: inner shell and outer (hydrophobic) shell. The inner interface shell contains the GMO $C_\beta-OH$ and $C_\gamma-OH$ bonds. The former has shown inert vibrational behavior upon increasing drug concentrations: its stretching frequency was around 1118 ± 1 cm^{-1}. In contrast, $C_\gamma-OH$ displayed different behavior upon drug incorporation. With initial drug content (1−2 wt %), the $C_\gamma-OH$ band kept constant at 1049 cm^{-1}, but with 3−4 wt % of GBP solubilized, an additional peak appeared at 1053.5 cm^{-1}, corresponding to the observed lamellar mesophase. At higher drug concentrations (5−10 wt %), the original peak disappeared, whereas the additional peak shifted downward by 1 cm^{-1}. These results imply a bond length deviation in comparison to the empty H_{II} system. Apparently, guest molecule polar interaction with the GMO hydroxyls caused a strength deviation of the $C_\gamma-OH$ bond. In addition, some of the $C_\gamma-OH$ groups are intramolecularly H-bonded to the surfactant's carbonyl, whereas the others are screened by water and guest molecules.[23] The intramolecular H bound to the free carbonyl ratio has undergone changes, as will be discussed next.

The stretching frequencies of the monoolein carbonyls, free and intra H-bonded, remained unchanged at 1742 and 1723 cm^{-1}, respectively. However, the ratio between the two populations (calculated by multipeak Gaussian fitting[6]) increased upon GBP loadings (Figure 5) and peaked at a value of 8.4 at 2−3 wt % GBP. Nevertheless, at 4 wt % GBP, the ratio dropped to 6.4 and gradually decreased. These results indicate enhanced hydrogen bonding within the interface region at low drug loads (1−3 wt %), coinciding with the observed tighter packed structures as measured by SAXS. This behavior is probably due to additional polar interactions of the drug's amine and carboxylate groups with monoolein's $C_\gamma-OH$ and carbonyls. At higher GBP contents, the interfacial area reached hydrogen bonding saturation. Partial H-bonding and cleavage of the GMO carbonyl took place,

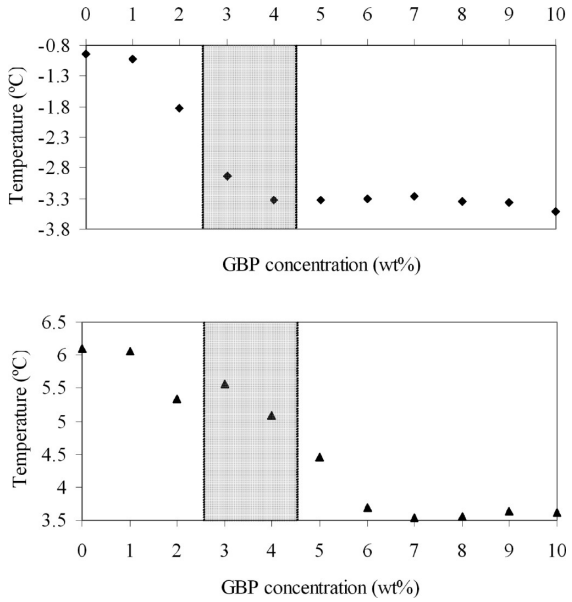

Figure 6. (a) T_m of H_2O and (b) T_m of the eutectic mixture, as a function of gabapentin content.

stabilizing the additional drug incorporation within the structure. Apparently, the drug further advanced toward the surfactant outer hydrophobic interface. At higher concentrations (5−10 wt %), the ratio decreased slightly more, corresponding to the lamellar structure and to the exposure of additional γ-OH bonding with its surroundings.

Another vibrational alteration was found in the ester's CO−O stretching frequency band, which increased from 1178 of the empty H_{II} to an average of 1180.8 ± 0.3 cm^{-1} upon increasing the GBP contents to 3 wt %. Then, at higher drug loads (4−10 wt %), the frequency progressively shifted downward to 1178.9 ± 0.5 cm^{-1}, exhibiting slight alterations, which are in line with the calculated H-bonded and free carbonyls ratio. According to Hubner and Mantsch, the effect may be associated with bond angle deviation of the dihedral angle as induced by torsional motions or by a small population of gauche conformers near the sn-1 ester single bond.[55] The authors demonstrated that red shifting of the CO−O band is in tune with a higher disorder state of the lipids. Indeed, GBP induced a tighter packed hexagonal structure with low drug loads of 1−3 wt % GBP (blue shifting), as was confirmed by SAXS analysis, and then, with higher drug loads (4−10 wt %), gabapentin induced a more loosely packed and disordered L_α structure (red shifting). With these surfactant interfacial vibrational frequencies data, we can assume that upon increasing gabapentin loads the ester group underwent hydrogen bond cleavage and bond angle deviation alterations to form and stabilize the lamellar structure.

Lipid-rich region represents the hydrophobic methylene chains. Their vibrational symmetric and asymmetric stretching frequencies have shown inert (noninfluenced) behavior with increasing concentrations of GBP and remained constant at 2853 and 2923 cm^{-1}, respectively (data not shown). It seems that the lipophilic region was not affected by GBP incorporation. To ensure or invalidate this observation, DSC analysis was applied.

DSC Analysis. To further comprehend molecular interactions induced by gabapentin, in particular, upon the lipid domains, DSC analysis was performed. Two endothermic minima were detected for the empty H_{II} system as reported by our earlier studies.[24] The fusion of the water molecules was ascribed to endotherm A and peaked at −0.91 °C. Peak B is ascribed to the melting of the GMO + tricaprylin tails of their eutectic mixture and was obtained at 6.1 °C.

GBP incorporation resulted in dropdown of T_m of both peaks by 2.5 °C. At low drug contents (1−4 wt %), the melting point of the water was primarily affected, exhibiting concentration-dependent behavior (Figure 6a). On the other hand, at high drug concentrations (4−7 wt %), the T_m of the lipid mixture was affected more than that of H_2O and found to be concentration-dependent (Figure 6b). In addition, fusion enthalpy of the water had a significant decrease of 30% (from 35 to 23 J g^{-1}) at low drug loads and a moderate decrease of 15% at high drug loads (29 J g^{-1}).

Combined with the ATR−FTIR results and the SAXS analysis, it can be inferred that in low drug loads the guest molecule was intercalated between the GMO headgroups and their aqueous environment. Competition for water binding was detected between GBP and GMO. Partial dehydration of the lipid polar heads was noticed in favor of hydrogen bonding between the drug's polar protonated amine and carboxylate and water. At increased loadings of the drug, GBP molecules were localized further, more toward the surfactant interface. This caused a gradual disorder in the lipid arrangement by spatial torsion forces on the interface curvature until the tightly packed and rigid hexagonal structure collapsed to form a much loosened lamellar structure, as observed by SAXS measurements. Finally, above the drug maximum solubilization capacity (7−10 wt %), where GBP crystals appeared, the lipid chains were no longer sterically affected, as implied by the observed near constant melting point of the eutectic mixture.

Interrelation between the Macroscopic Behavior of the GBP-Modified Mesophases and Their Molecular Level Interactions. *Rheology.* Rheological measurements were implemented to evaluate the viscoelastic properties of the GBP solubilized into LLC systems and to correlate these mesophases' molecular structure and interactions to macroscopic mechanical properties.[11] Frequency-dependent measurements were conducted to determine the storage modulus $G'(\omega)$, loss modulus $G''(\omega)$, complex viscosity η^*, and maximum relaxation time τ_{max}. In our previous reports, a typical oscillatory sweep curve's behavior of the empty H_{II} system was demonstrated.[6,10,11] Herein, only samples with solubilized drug (0−6 wt % GBP) were investigated. In the range of the homogeneous hexagonal mesophases (0−2 wt % GBP), a similar tendency was observed and will be discussed first. According to the Maxwell model, which is described elsewhere and generally applies to H_{II} systems,[31] the longest relaxation time (τ_{max}) is calculated as the reciprocal frequency at the crossover point of the storage and loss moduli ($1/\omega$). τ_{max} is an inherent property of a Maxwell viscoelastic material, which describes the time window required for the lipid−water interface to equilibrate back to the initial (thermodynamically stable) configuration upon shear perturbation. Beneath the intersection, at lower frequencies the values of the storage modulus are lower than those of the loss modulus. This means that the loss energy, which is stated as the viscous forces of the LLC microstructure, exceeds the stored energy, which is stated as the elastic forces of the assembly. Therefore, up to the crossover point, the system is more viscous than elastic. Around the crossover point, the microstructure possesses viscoelastic properties classified by Mezzenga et al. as "the transition to the flow region",[18] and at higher frequencies, above the

Table 1. Summary of the Longest Relaxation Time (τ_{max}), Zero-Shear Viscosity (η_0), Gel Strength (S), and Relaxation Exponent (m), As Affected by Increasing Gabapentin Content

GBP (wt %)	τ_{max} (s)	η_0 (Pa s)	S	m
0	1.06	18316	12256	−0.53
1	1.81	21396	11289	−0.57
2	1.97	53387	26328	−0.69
3			17525	−0.67
4			6988	−0.65

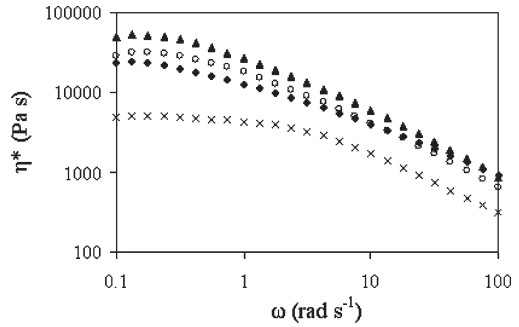

Figure 7. Complex viscosity as a function of the applied oscillation frequency for the following gabapentin contents (wt %): ♦, 0; ▲, 2; ○, 3; ×, 4.

crossover point, the trend turns over: $G' > G''$, the system is more elastic. Likewise, the observed experimental dynamic moduli behavior suits the following quasi-Maxwellian frequency dependence functions.

$$G'(\omega) = \frac{\omega^2\tau\eta_0}{1+(\omega\tau)^2};\ G''(\omega) = \frac{(\omega\eta_0)}{1+(\omega\tau)^2}$$

These equations imply that at high angular frequencies the storage modulus (G') should reach a plateau value while the dissipative modulus (G'') should pass through a maximum. It should be mentioned that the system follows the Maxwell model in frequencies lower than the crossover point, where the plot G'/G'' represents a straight line.[56]

The longest relaxation time of samples with 0−2 wt % GBP, summarized in Table 1, demonstrated that τ_{max} increased with 1 wt % gabapentin and peaked to a merely 2-fold value of 1.97 s with 2 wt % of the drug incorporated, reflecting a more elastic response. Reinforcement of the observed trend was obtained by plotting the complex viscosity of these samples (and samples containing 3−4 wt % GBP) versus the oscillation frequency. As seen in Figure 7, all samples possessed a shear thinning behavior typical of viscoelastic materials. η^* exhibited a constant value as a result of the LLC domains rearrangement in the flow direction, due to entanglements and interactions between them. This plateau is described as the zero-shear viscosity (η_0) and suits a typical viscoelastic material, regardless of its composition. In the homogeneous H_{II} mesophases (0−2 wt % GBP), η_0 can be evaluated by the crossover point of the dynamic moduli,[57] $\eta_0 = 2G'(\omega)\tau_{max}$. The zero-shear viscosity of these samples is summarized in Table 1. η_0 reflects the strength of the intermolecular interactions within the assembly. Clearly, these interactions are extremely enhanced to a nearly 3-fold value with 2 wt % of guest molecules introduced into the LLC system (in comparison to the empty H_{II}), due to strong polar interactions induced by GBP within the hydrophilic moieties of the surfactant and their environment.

As frequency increases, the domains progressively reorient and coalign perpendicular to the oscillation applied. At high frequencies, the oriented domains are squashed to form a quasi monodomain, demonstrating a shear thinning behavior that may be explained by the slip-plane theory introduced by Radiman et al. to comprehend relaxation in weak solids.[58] Qualitatively, η^* peaked with 2 wt % GBP, and gradually declined to a minimum with 4 wt % GBP. To quantify this behavior, the power law model was applied, $\eta^* = S\omega^b$,[56] where S is the gel strength, estimated by the intermolecular interactions and b is the relaxation exponent, indicating "solid-like" and "liquid-like" responses when approaching −1 and 0, respectively. The empty system exhibits nearly pure viscoelastic properties (in which $b = -0.5$), while 2 wt % GBP induced a maximal solid-like response with a corresponding 2.4-fold increase in S value (Table 1). With 4 wt % GBP, S dropped to half the value of the empty H_{II}, and b slightly reduced as well. These results are in line with the SAXS measurements. As shown, the lattice parameter declined by 6 Å to a minimum with 2 wt % drug solubilized, meaning a more tightly packed cylindrical H_{II} structure with greater resistance to mechanical forces such as oscillated shearing. In addition, ATR−FTIR results showed strengthening of hydrogen bonding between the polar groups of the drug, the O−H headgroups of the GMO, and the water. These competitive hydrogen interactions caused the system to become more rigid with enhanced elasticity and greater complex viscosity. With the appearance of the lamellar mesophase (3−4 wt % of GBP), the dynamic moduli and complex viscosity gradually decreased, probably due to less ordered heterogeneous mesophases with increasing L_α content. Apparently, the drug reduced the interfacial curvature due to intercalation of its polar groups between the GMO headgroups, by sterically hindering and immobilizing their movement. Consequently, the interfacial dihedral angle of the ester group was spatially affected by the surfactant headgroups' deficient bending ability, resulting in declined curvature and less-ordered loosened-packed 1D lamellar domains. Thus, these systems exhibit weaker mechanical properties such as inferior dynamic moduli values and a more liquid-like response upon oscillated perturbation and shearing.

Samples with 5−6 wt % GBP possess a much narrower LVR region that merely reaches 10 Pa, indicating much weaker viscoelastic properties in comparison to the relatively stiff samples analyzed previously. Apparently, the randomly oriented monodomains consisting of many structural modifications caused by gabapentin within their lamellar microstructures contribute to the disoriented macroscopic appearance. The viscoelastic behavior of the two samples is drawn in Figure 8a,b. G' and G'' of a sample with 5 wt % GBP are 1 order of magnitude greater than those of 6 wt % GBP, indicating a more rigid system in comparison to the weaker system of 6 wt % GBP. In both samples, the dynamic moduli slightly decreased to a minimum at near-zero frequencies. Alfaro et al. explained this phenomenon by the formation of an elastic network due to interactions developing within the monodomains.[59] The phenomenon is more pronounced at 5 wt % GBP, where the minimum in the loss modulus occurs at 0.237 rad s^{-1}, suggesting a significant shear effect that is annotated by polarized light micrographs of before and after a relatively minuscule shearing (Figure 9a−f). The supporting findings demonstrate different textures observed for an uncovered slide and for the slip-covered slide (obtained by placing a cover on top of the sample). We can presume that the

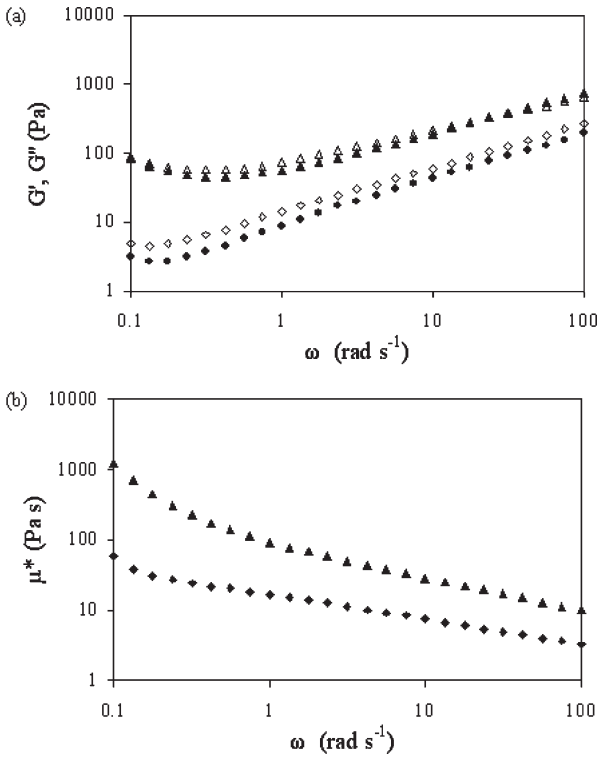

Figure 8. (a) Storage (filled signs) and loss (empty signs) moduli as a function of the applied oscillation frequency for gabapentin content of 5 wt % ▲, and 6 wt % ♦. (b) Complex viscosity as a function of the applied oscillation frequency for GBP content of 5 wt %, ▲, and 6 wt % ♦.

shear force induced by covering caused the vesicle-entangled lamellar domains to deform into a network of MLVs aligned on reoriented planar lamellae. Then, ULVs were formed and eventually collapsed to an isotropic micellar solution. Likewise, the complex viscosity of 5−6 wt % GBP dropped steeply in the low-frequency region (Figure 8b) following the decrease of the shear moduli.

As the oscillation rate increases, both dynamic moduli monotonically rise. The storage modulus curve fits a "weak gel-like" behavior in which $G'(\omega) = \omega^n$, where n is the relaxation exponent and ranges between 0 and 1, corresponding to solid-like and liquid-like responses relatively. Winter and De Rosa reasoned this kind of dynamic behavior by the self-similarity of the structure over a wide range of length scale, i.e., due to the mesophase fractal nature.[60] Indeed, lamellar mesophases were shown by birefringence patterns analysis to exhibit a fractal nature.[61] It should be mentioned that fractal properties of a material manifesting a large surface area may be attributed to drug delivery enhancement.[62] The relaxation exponent was found to be 0.51 and 0.87 for 5 and 6 wt % GBP samples, respectively, indicating that the 6 wt % GBP sample possesses a conspicuous liquid-like response. Likewise, at 5 wt % GBP, the moduli behaved almost identically ($G' \approx G'' \approx \omega^n$). An identical pattern was observed for a diamond cubic LLC system composed of didodecyldimethylammonium bromide (DDAB)/D_2O/toluene at the system's melting point.[63] Additional rheological information was obtained by analyzing the complex viscosity as depicted in the mid0 and high-frequency regions (Figure 8b). The power law model was applied for the 5 wt % GBP in the midrange oscillation rate (up to $\omega < 7.5$ rad s^{-1}), with S and b values of 98.2 and −0.68, respectively. Then, in the higher-frequency region, both values dropped to $S = 83.6$ and $b = -0.43$, which can be explained by an initial deformation of the oriented (MLVs containing) lamellar network into a form of lamellae containing smaller MLVs, accompanied by instant formation of ULVs with somewhat resistance to the applied oscillated shear perturbation. Ultimately, the dispersed lamellae and ULVs are broken into a micellar isotropic liquid. A similar trend was observed for the 6 wt % GBP, where the gel strength parameter and the relaxation exponent were consistent in the mid- to high-frequency regions, with reduced values of $S = 16.4$ and $b = -0.34$, respectively, corresponding to a comprehensive and swift deformation of the weakly bounded network into a micellar solution with obvious liquid-like response. From DSC analysis, we can assume that at 6 wt % GBP the disordered state of the lipids within the hydrophobic moiety is more pronounced in comparison to 5 wt % of drug solubilized. The ATR−FTIR results coincide with this assumption. The ratio of the H-bound to "free" carbonyl of the GMO interfacial ester decreased in the 6 wt % GBP sample, implying a higher level of steric hindrance and disorder at the interface area. The outcome is a more loosely packed mesophase with inferior ability to resist mechanical disturbances.

In the present work, as well as others,[10,18] rheology is an important analytical tool for distinguishing closely related, nevertheless different, liquid crystalline mesophases. These similar mesophases exhibited the same polarized light micrographs and SAXS d-spacing peak patterns. Distinction was achieved due to different rheological behaviors, which were reinforced by additional spectroscopic and thermal analyzing methods such as ATR−FTIR and DSC.

Transdermal Delivery of Gabapentin—In Vitro Studies. Preliminary transdermal permeation evaluation of GBP was carried out through an in vitro system of Franz diffusion cells. Drug permeability was examined via formulations of H_{II}, L_α, and a reference aqueous solution containing 2, 6, and 10 wt % gabapentin. The mesophases' existence at body temperature was validated by SAXS measurements prior to the transdermal experiments. The lattice parameter of H_{II} dropped by 3 Å, compared to the one measured at $T = 25$ °C, perhaps as a result of better packing of the lipids.[31] In contrast, $\alpha(L_\alpha)$ modestly decreased by 1 Å, assumingly due to the already disordered state of the interface, which prevented a tighter packing of the lipids. Characteristic profiles of the cumulative drug permeation (Q_t) per unit of skin surface area of GBP from the different mesophases and the aqueous solution are shown in Figure 10. The quantity of drug crossing the skin via the hexagonal and the defected lamellar mesophases in a period of 24 h was 1.107 and 1.896 mg cm^{-2}, respectively, and was profoundly slower, compared to the water solution ($Q_{t=24} = 4.596$ mg cm^{-2}). Likewise, the steady-state fluxes (J_{ss}) were calculated in the observed linear range of 6−24 h after loading time. A similar tendency was obtained for the different carriers' fluxes, where the aqueous solution flux ($J_{ss} = 252.27\ \mu g\ h^{-1}\ cm^{-2}$) was found to be 4.2- and 2.5-fold higher than the H_{II} and L_α mesophases' fluxes. These results clearly show that within a day the LLC vehicles sustained the gabapentin permeation rate and cumulative pass, in comparison to the water.

The mechanism by which a drug infiltrates the skin is subject to several factors such as the molecule's chemical and spatial nature, its size, and the operating vehicle from which the drug is released. Apparently, for small hydrophilic compounds, the applied vehicle governs the preferred penetrating pathway. By

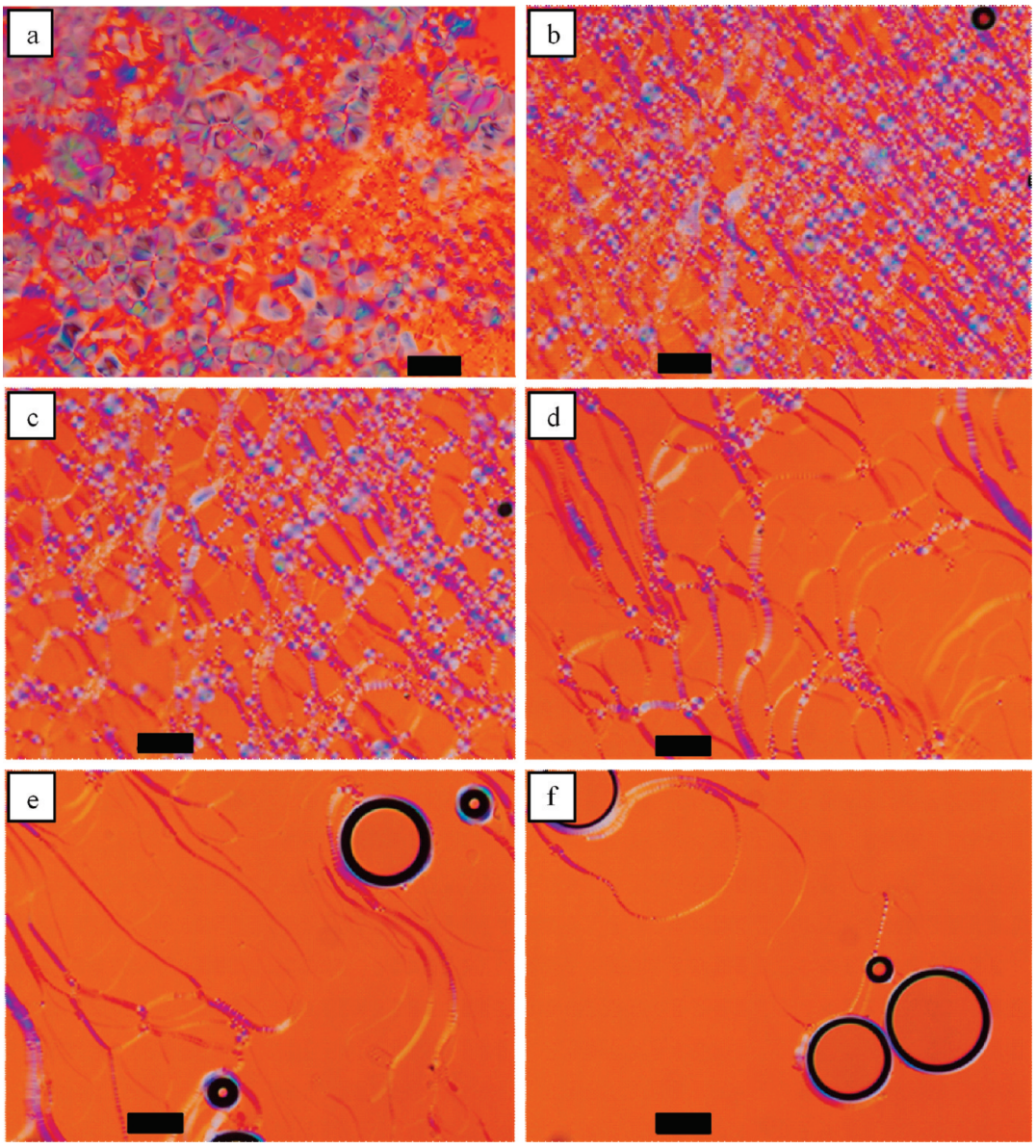

Figure 9. Cross-polarized light microscope texture obtained for (a) the uncovered slide and (b) immediately, (c) 2 min, (d) 5 min, (e) 8 min, and (f) 15 min after placing a cover. The scale bar is 100 μm.

utilizing two-photon microscopy (TPM) with (SFB), Bender et al. demonstrated different carrier-dependent penetration pathways for the hydrophilic fluorescent marker.[64] The dominant pathway for the marker's diffusion via the water was the intercellular lipid matrix. In contrast, by using a bicontinuous cubic LLC carrier based on either phytantriol or GMO, the marker diffused predominantly through the corneocytes' intercluster pathway prior to its infiltration to the underneath intercellular matrix. In the intercluster pathway, the fluorescent dye was found to reside in the skin's microfissures and in a three-dimensional network of thin threads. The authors attributed this kind of sustained release behavior to the relatively high elasticity of the LLCs and to their lipids' ability to interact with the intercellular lipid matrix. Likewise, in a study of the transdermal penetration pathway of liposomes, van Kuijk-Meuwissen et al. showed by using confocal laser scanning microscopy (CLSM) that the penetration depth of liposomes is governed by the flexibility of their bilayers—greater flexibility resulting in deeper depth of penetration.[65] The authors also concluded that higher deformability of the lamellar vesicles increases the infiltration ability as well.

It is deducible from these interpretations that in the present case the LLC carriers delivered the drug in a similar pattern. It seems that the sustained release of gabapentin was achieved using the hexagonal mesophase. It delayed gabapentin permeation into the microfissures in a most significant way, primarily due to its high elasticity. An additional factor that contributes to the sustained release behavior is the tightly packed structure induced by GBP intercalation within the water rods interface, which was achieved by pronounced hydrogen bonding interactions with the surfactant headgroups and their water surroundings. In a more moderated way, the defected lamellar mesophase was able to sustain the percutaneous diffusion as well, compared to the reference water solution. However, inferior viscoelastic properties and structural defects (local lipid reorganizations and MLVs existence) caused by high gabapentin content within increased the lamellar mesophase's ability to penetrate deeper into the skin

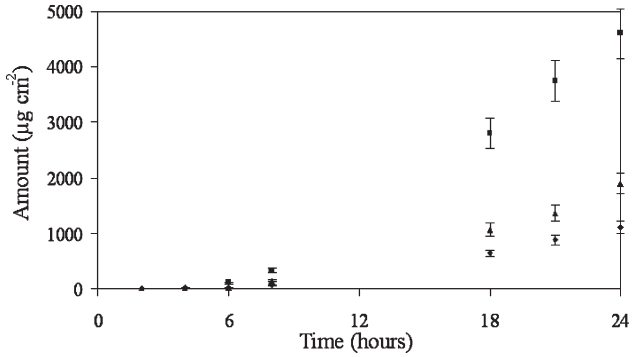

Figure 10. Cumulative transdermal penetration of gabapentin via the different carriers: water solution (10 wt % GBP) ■; lamellar (6 wt % GBP) ▲; H_{II} (2 wt % GBP) ♦.

layers with enhanced delivery, compared to the hexagonal one. It should be noted that the drug diffusion from both LLC vehicles occurs partially thanks to adequate structural properties of LLCs in the microscopic range (as indicated by the lattice parameter) and in the mesoscopic range (as expressed by alignment of discontinuous and anisotropic polycrystalline domains, possessing fractal characteristics).[23] Clearly, further comprehensive research regarding the percutaneous penetration mechanism of bioactive molecules via varying carriers is required, in particular, the understanding of diffusion pathways of hydrophilic drugs through LLCs carriers, in more precise and detailed analyzing techniques.

CONCLUSIONS

In the current study, we investigated the structural alterations and molecular interactions caused by introduction of gabapentin into GMO-based H_{II} mesophases. The drug maximum solubilization capacity and its location within the concentration-dependent mesophases were examined as well. The GBP percutaneous permeation rate via the modified LLCs was demonstrated.

Structural characterization has shown that gabapentin induced a $H_{II}-L_{\alpha}$ transition, while its maximum solubility capacity was achieved at 6 wt %, resulting in a defective and modified lamellar structure. The hexagonal symmetry was maintained up to 2 wt % GBP; nonetheless, at this GBP content, the lattice parameter significantly decreased by 6 Å. ATR−FTIR results indicated enhanced hydrogen bonding between the polar groups of the guest molecule (especially the protonated amine) and the O−H groups of the GMO and their water surrounding in the inner hydrophilic interface region. At phase transition concentrations of 3−4 wt % GBP, the outer hydrophobic interface region was extremely altered, as reflected by the peak of the H-bonded carbonyl population at 3 wt %, followed by a drastic drop at 4 wt %. The esteric dihedral angle was spatially affected as well. At 5−6 wt % GBP, lamellar structures were obtained. However, these mesophases possessed local structural defects such as lipid rearrangements and existence of MLVs, as was inferred from cross-polarized light microscopy. In addition, DSC analysis revealed a gradual disorder increase within the lipid arrangement, especially at higher drug loads of 4−6 wt %, probably as a result of the spatially altered interface area.

Rheological measurements reinforced the trend obtained with increasing GBP content. Elasticity was enhanced within the homogeneous hexagonal mesophases and peaked at 2 wt % GBP with increased solid-like response. The elasticity progressively decreased at moderate drug loads of 3−4 wt %, whereas the liquid-like response increased. Greater guest molecule contents of 5−6 wt % were found to possess a pronounced liquid-like response and deteriorated elasticity. Moreover, by rheological means, we were able to differentiate the two mesophases; at 5 wt % GBP, a more rigid system was identified, whereas at maximum solubilization capacity the mesophase was found to be the most fluidic one with inferior viscoelastic properties, interrelating to the highest degree of disorder within that mesophase.

Ultimately, the drug-loaded mesophases displayed sustained-release behavior upon in vitro transdermal delivery of gabapentin in comparison to the reference aqueous solution. Likewise, a correlation between the applied mesophase and its transdermal penetration profile was demonstrated, such that the hexagonal structure was shown to be the most efficient carrier for sustained delivery while the lamellar one delayed the release in a more moderate way.

The results presented in this work can be wisely exploited to easily produce gabapentin concentration and flux-dependent formulations based on GMO to treat a variety of neural disorders by percutaneous administration. Further temperature-dependent examination of the solubilized mesophases is required. On a final note, there are several GBP analogues (some in use[66] while the others are still under research[67]) that may act in a similar physicochemical manner when introduced to the H_{II} system and thus could be utilized as well.

AUTHOR INFORMATION

Corresponding Author

*Tel.: 972-2-6586574/5. Fax: 972-2-6520262. E-mail: garti@vms.huji.ac.il.

REFERENCES

(1) Bender, F.; Chilcott, T. C.; Coster, H. G. L.; Hibbert, D. B.; Gooding, J. J. *Electrochim. Acta* **2007,** *52*, 2640–2648.
(2) Strom, P. *J. Colloid Interface Sci.* **1992,** *154*, 184–193.
(3) Landau, E. M.; Rosenbusch, J. P. *Proc. Natl. Acad. Sci. U.S.A.* **1996,** *96*, 14532–14535.
(4) Cherezov, V.; Clogston, J.; Papiz, M. Z.; Caffrey, M. *J. Mol. Biol.* **2006,** *357*, 1605–1618.
(5) Sagalowicz, L.; Leser, M. E.; Watzke, H. J.; Michel, M. *Trends Food Sci. Technol.* **2006,** *17*, 204–214.
(6) Mishraki, T.; Libster, D.; Aserin, A.; Garti, N. *Colloids Surf. B* **2010,** *75*, 47–56.
(7) Boyd, B. J.; Whittaker, D. V.; Khoob, S. M.; Davey, G. *Int. J. Pharm.* **2006,** *309*, 218–226.
(8) Efrat, R.; Kesselman, E.; Aserin, A.; Garti, N.; Danino, D. *Langmuir* **2009,** *25*, 1316–1326.
(9) Amar-Yuli, I.; Aserin, A.; Garti, N. *J. Phys. Chem. B* **2008,** *112*, 10171–10180.
(10) Libster, D.; Aserin, A.; Yariv, D.; Shoham, G.; Garti, N. *J. Phys. Chem. B* **2009,** *113*, 6336–6346.
(11) Libster, D.; Aserin, A.; Wachtel, E.; Shoham, G.; Garti, N. *J. Colloid Interface Sci.* **2007,** *308*, 514–524.
(12) Kraineva, J.; Nicolini, C.; Thiyagarajan, P.; Kondrashkina, E.; Winter, R. *Biochim. Biophys. Acta* **2006,** *1764*, 424–433.
(13) Lendermann, J.; Winter, R. *Phys. Chem. Chem. Phys.* **2003,** *5*, 1440–1450.
(14) Leslie, S. B.; Puvvada, S.; Ratna, B. R.; Rudolph, A. S. *Biochim. Biophys. Acta* **1996,** *1285*, 246–254.
(15) Sadhale, Y.; Shah, J. C. *Int. J. Pharm.* **1999,** *191*, 51–64.
(16) Prouzet, E.; Brubach, J.-B.; Roy, P. *J. Phys. Chem. B* **2010,** *114*, 8081–8088.

(17) Drummond, C. J.; Fong, C. *Curr. Opin. Colloid Interface Sci.* **2000,** *4*, 449–456.
(18) Mezzenga, R.; Meyer, C.; Servais, C.; Romoscanu, A. I.; Sagalowicz, L.; Hayward, R. C. *Langmuir* **2005,** *21*, 3322–3333.
(19) Larsson, K. *J. Phys. Chem.* **1989,** *93*, 7304–7314.
(20) Qiu, H.; Caffrey, M. *Biomaterials* **2000,** *21*, 223–234.
(21) Efrat, R.; Abramov, Z.; Aserin, A.; Garti, N. *J. Phys. Chem. B* **2010,** *114*, 10709–10716.
(22) Ben Ishai, P.; Libster, D.; Aserin, A.; Garti, N.; Feldman, Y. *J. Phys. Chem. B* **2009,** *113*, 12639–12647.
(23) Libster, D.; Ben Ishai, P.; Aserin, A.; Shoham, G.; Garti, N. *Langmuir* **2008,** *24*, 2118–2127.
(24) Amar-Yuli, I.; Wachtel, E.; Ben Shoshan, E.; Danino, D.; Aserin, A.; Garti, N. *Langmuir* **2007,** *23*, 3637–3645.
(25) Jin, A. J.; Nossal, R. *Biophys. J.* **1993,** *65*, 1523–1537.
(26) Cheng, Y.; Boll, W.; Kirchhausen, T.; Harrison, S. C.; Walz, T. *J. Mol. Biol.* **2007,** *365*, 892–899.
(27) Larsson, K.; Fontell, K.; Krog, N. *Chem. Phys. Lipids* **1980,** *27*, 321–328.
(28) Amar-Yuli, I.; Libster, D.; Aserin, A.; Garti, N. *Curr. Opin. Colloid Interface Sci.* **2009,** *14*, 21–32.
(29) Cohen-Avrahami, M.; Aserin, A.; Garti, N. *Colloids Surf. B* **2010,** *77*, 131–138.
(30) Amar-Yuli, I.; Garti, N. *Colloids Surf. B* **2005,** *43*, 72–82.
(31) Amar-Yuli, I.; Wachtel, E.; Shalev, D. E.; Moshe, H.; Aserin, A.; Garti, N. *J. Phys. Chem. B* **2007,** *111*, 13544–13553.
(32) Libster, D.; Ben Ishai, P.; Aserin, A.; Shoham, G.; Garti, N. *Int. J. Pharm.* **2009,** *367*, 115–126.
(33) Silvenius, J.; Kalviainen, R.; Ylinen, A.; Riekkinen, P. *Epilepsia* **1991,** *32*, 539–542.
(34) Rowbotham, M.; Harden, N.; Stacey, B.; Bernstein, P.; Magnus-Miller, L. *JAMA* **1998,** *280*, 1837–1842.
(35) Rosenberg, J. M.; Harrell, C.; Ristic, H.; Werner, R. A.; deRosayro, A. M. *Clin. J. Pain* **1997,** *13*, 251–255.
(36) Backonja, M.; Beydoun, A.; Edwards, K. R.; Schwartz, S. L.; Fonseca, V.; Hes, M.; LaMoreaux, L.; Garofalo, E. *JAMA* **1998,** *280*, 1831–1836.
(37) Guttuso, T. J.; Kurlan, R.; McDermott, M. P.; Kieburtz, K. *Obstet. Gynecol.* **2003,** *101*, 337–345.
(38) Garcia-Borreguero, D.; Larrosa, O.; de la Llave, Y.; Verger, K.; Masramon, X.; Hernandez, G. *Neurology* **2002,** *59*, 1573–1579.
(39) Pollack, M. H.; Matthews, J.; Scott, E. L. *Am. J. Psychiatry* **1998,** *155*, 992–993.
(40) Corbett, J. *Curr. Neurol. Neurosci. Rep.* **2007,** *7*, 395–396.
(41) McLean, R.; Proudlock, F.; Thomas, S.; Degg, C.; Gottlob, I. *Ann. Neurol.* **2007,** *61*, 130–138.
(42) Myrick, H.; Malcolm, R.; Randall, P. K.; Boyle, E.; Anton, R. F.; Becker, H. C.; Randall, C. L. *Alcohol.: Clin. Exp. Res.* **2009,** *33*, 1582–1588.
(43) Bozikas, V.; Petrikis, P.; Gamvrula, K.; Savvidou, I.; Karavatos, A. *Prog. Neuropsychopharmacol. Biol. Psychiatry* **2002,** *26*, 197–199.
(44) Gee, N. S.; Brown, J. P.; Disanayake, V. U. K.; Offord, J.; Thurlow, R.; Woodruff, G. N. *J. Biol. Chem.* **1996,** *271*, 5768–5776.
(45) Marais, E.; Klugbauer, N.; Hofmann, F. *Mol. Pharmacol.* **2001,** *59*, 1243–1248.
(46) Brown, J. T.; Randall, A. *Synapse* **2005,** *55*, 262–269.
(47) Uchino, H.; Kanai, Y.; Kim do, K.; Wempe, M. F.; Chairoungdua, A.; Morimoto, E.; Anders, M. W.; Endou, H. *Mol. Pharmacol.* **2002,** *61*, 729–737.
(48) Stewart, B. H.; Kugler, A. R.; Thompson, P. R; Bockbrader, H. N. *Pharm. Res.* **1993,** *10*, 276–281.
(49) McLean, M. J. *Epilepsia* **1995,** *36*, S73–S86.
(50) Rice, A. S.; Maton, S. *Pain* **2001,** *94*, 215–224.
(51) Hernandez, B.; Pfluger, F.; Nsangou, M; Ghomi, M. *J. Phys. Chem. B* **2009,** *113*, 3169–3178.
(52) Jalalizadeh, H.; Souri, E.; Tehrani, M. B.; Jahangiri, A. *J. Chromatogr. B* **2007,** *854*, 43–47.
(53) Efrat, R.; Aserin, A.; Garti, N. *J. Colloid Interface Sci.* **2008,** *321*, 166–176.
(54) Israelachvili, J. N.; Mitchell, D. J.; Ninham, B. W. *J. Chem. Soc.* **1976,** *72*, 1525–1568.
(55) Hubner, W.; Mantsch, H. H. *Biophys. J.* **1991,** *59*, 1261–1272.
(56) Nemeth, Z.; Halasz, L.; Palinkas, J.; Bota, A.; Horanyi, T. *Colloids Surf. A* **1998,** *145*, 107–119.
(57) Siddig, M. A.; Radiman, S.; Jan, L. S.; Muniandy, S. V. *Colloids Surf. A* **2006,** *276*, 15–21.
(58) Radiman, S.; Toprakcioglu, C.; McLeish, T. C. B. *Langmuir* **1994,** *10*, 61–67.
(59) Alfaro, M. C.; Guerrero, A. F.; Munoz, J. *Langmuir* **2000,** *16*, 4711–4719.
(60) De Rosa, M. E.; Winter, H. H. *Rheol. Acta* **1994,** *33*, 220–237.
(61) Muniandy, S. V.; Kan, C. S.; Lim, S. C.; Radiman, S. *Phys. A* **2003,** *323*, 107–123.
(62) Yariv, D.; Efrat, R.; Libster, D.; Aserin, A.; Garti, N. *Colloids Surf. B* **2010,** *78*, 185–192.
(63) Jones, J. L.; McLeish, T. C. B. *Langmuir* **1999,** *15*, 7495–7503.
(64) Bender, J.; Simonsson, C.; Smedh, M.; Engstrom, S.; Ericson, M. B. *J. Controlled Release* **2008,** *129*, 163–169.
(65) van Kuijk-Meuwissen, M. E.; Junginger, H. E.; Bouwstra, J. A. *BBA* **1998,** *1371*, 31–39.
(66) Dworkin, R. H.; Kirkpatrick, P. *Nat. Rev. Drug Discovery* **2005,** *4*, 455–456.
(67) Blakemore, D. C.; Bryans, J. S.; Carnell, P.; Chessum, N. E. A.; Field, M. J.; Kinsella, N.; Kinsora, J. K.; Osborne, S. A.; Williams, S. C. *Bioorg. Med. Chem. Lett.* **2009,** *20*, 248–251.